Amino Acids (2011) 41:1233–1245
DOI 10.1007/s00726-010-0801-2

ORIGINAL ARTICLE

Role of low native state kinetic stability and interaction of partially unfolded states with molecular chaperones in the mitochondrial protein mistargeting associated with primary hyperoxaluria

Angel L. Pey · Eduardo Salido · Jose M. Sanchez-Ruiz

Received: 12 July 2010 / Accepted: 28 October 2010 / Published online: 20 November 2010

Abstract The G170R variant of the alanine:glyoxylate aminotransferase (AGT) is the most common pathogenic allele associated to primary hyperoxaluria type I (PH1), leading to mitochondrial mistargeting when combined with the P11L and I340M polymorphisms (*minor allele*; AGT_{LM}). In this work, we have performed a comparative analysis on the conformation, unfolding energetics and interaction with molecular chaperones between AGT_{wt}, AGT_{LM} and AGT_{LRM} (G170R in the minor allele) proteins. Our results show that these three variants share similar conformational and functional properties as folded dimers. However, kinetic stability analyses showed a $\approx$1,000-fold increased unfolding rate for apo-AGT_{LRM} compared to apo-AGT_{wt}, as well as a reduced folding efficiency upon expression in *Escherichia coli*. Pyridoxal 5′-phosphate (PLP)-binding provided a 4–5 orders of magnitude enhancement of the kinetic stability for all variants, suggesting a role for kinetic stabilization in pyridoxine-responsive PH1. Conformational studies at mild acidic pH and moderate guanidium concentrations showed the formation of a molten-globule-like unfolding intermediate in all three variants, which do not reactivate to the native state and strongly interact with Hsc70 and Hsp90 chaperones. Additional expression analyses in a mammalian cell-free system at neutral pH showed enhanced interaction of AGT_{LRM} with Hsc70 and Hsp90 proteins compared to AGT_{wt}, suggesting kinetic trapping of the mutant by chaperones along the folding process. Overall, our results suggest that mitochondrial mistargeting of AGT_{LRM} may involve the presentation of AGT partially folded states to the mitochondrial import machinery by molecular chaperones, which would be facilitated by the low native state kinetic stability (partially corrected by PLP binding) and kinetic trapping during folding of the AGT_{LRM} variant with molecular chaperones.

Keywords Alanine:glyoxylate aminotransferase · Protein kinetic stability · Partially folded states · Molecular chaperones · Primary hyperoxaluria type 1

Abbreviations

AGT	Alanine:glyoxylate aminotranferase
ANS	8-Anilinonaphthalene-1-sulfonic acid
CD	Circular dichroism
DSC	Differential scanning calorimetry
PH1	Primary hyperoxaluria type 1
PLP	Pyridoxal 5′-phosphate
SEC	Size-exclusion chromatography

Introduction

Human peroxisomal alanine:glyoxylate aminotransferase (hAGT; E.C. 2.6.1.44) is a pyridoxal 5′-phosphate (PLP) dependent enzyme that catalyzes the transamination of the intermediate metabolite glyoxylate to glycine (Danpure

Electronic supplementary material The online version of this article (doi:10.1007/s00726-010-0801-2) contains supplementary material, which is available to authorized users.

A. L. Pey (✉) · J. M. Sanchez-Ruiz
Departamento de Química-Física, Facultad de Ciencias, Universidad de Granada, 18071 Granada, Spain
e-mail: angelpey@ugr.es

E. Salido
Hospital Universitario Canarias, Center Biomedical Research on Rare Diseases (CIBERER) and Institute of Biomedical Technologies (ITB), Tenerife, Spain

2006). Functional deficiency of hAGT activity leads to accumulation of glyoxylate in peroxisomes, which is consequently transported to the cytosol and oxidized to oxalate. Deficiency in hAGT activity causes primary hyperoxaluria type I (PH1), a rare autosomal inborn error of metabolism (around 1 in 120,000 newborns) characterized by progressive renal failure due to accumulation of insoluble calcium oxalate (Danpure 2006; Williams et al. 2009). The most successful treatment or cure for PH1 is a combined liver and kidney transplantation. However, partial correction of PH1 is found for some specific genotypes (such as G170R) by administration of the PLP precursor, pyridoxine (Danpure 2006). About 150 mutations in the *AGXT* gene have been described, 50% of them being missense mutations (Williams et al. 2009). There exists one common polymorphic variant called minor allele (AGT_{LM}; ~20% in control subjects and ~46% in PH1 patients), which contains two single aminoacid substitutions (P11L and I340M) among other genomic substitutions (Williams et al. 2009).

The molecular mechanisms underlying the functional defect of AGT caused by PH1 variants may involve mistargeting or misfolding depending on the AGT variant (Williams et al. 2009). Mistargeting leads to mitochondrial transport of AGT proteins, where the enzyme is metabolically inefficient, while misfolding is associated to a reduced ability of AGT protein to fold into native dimers causing enhanced protein aggregation and/or degradation (Danpure 2006; Lumb and Danpure 2000; Santana et al. 2003; Williams et al. 2009). In both scenarios, the minor allele plays a role. It creates a functionally weak mitochondrial targeting sequence that allows mitochondrial import into isolated mitochondria, but requires additional mutations to manifest significant mistargeting intracellularly (Motley et al. 1995; Purdue et al. 1991). In addition, the minor allele increases the sensitivity of native dimers towards thermal and chemical unfolding (Cellini et al. 2009; Hopper et al. 2008). Since some PH1 mutations are affecting the kinetic partitioning of AGT protein between folding into native dimers and peroxisomal import, mistargeting into mitochondria and cytosolic/peroxisomal degradation, molecular chaperones and other factors (such as degradation machinery and effector proteins) must play a role on the final fate of AGT variants intracellularly [see (Bukau and Horwich 1998; Martinez et al. 2008)].

In this work we have characterized the conformation and stability of three hAGT variants (AGT_{wt}, AGT_{LM} and AGT_{LRM}; see Fig. 1 for the location of the mutated residues in the three-dimensional structure of AGT_{wt}) under native and partially unfolding conditions. We show that the three hAGT variants display similar overall conformation and function (activity and PLP binding affinities) but the minor allele variants (AGT_{LM} and AGT_{LRM}) display substantially lower kinetic stability than the wt protein (major allele), while PLP binding strongly enhances kinetic stability in all three protein variants. Interestingly, at mild acidic conditions ($pH < 5$) all three hAGT variants form an inactive unfolding intermediate resembling a *molten globule* state, characterized by high residual secondary structure, solvent-protected intrinsic fluorophores, enhanced binding of the hydrophobic dye 8-anilinonaphthalene-1-sulfonic acid (ANS) and increased conformational flexibility. Experiments performed

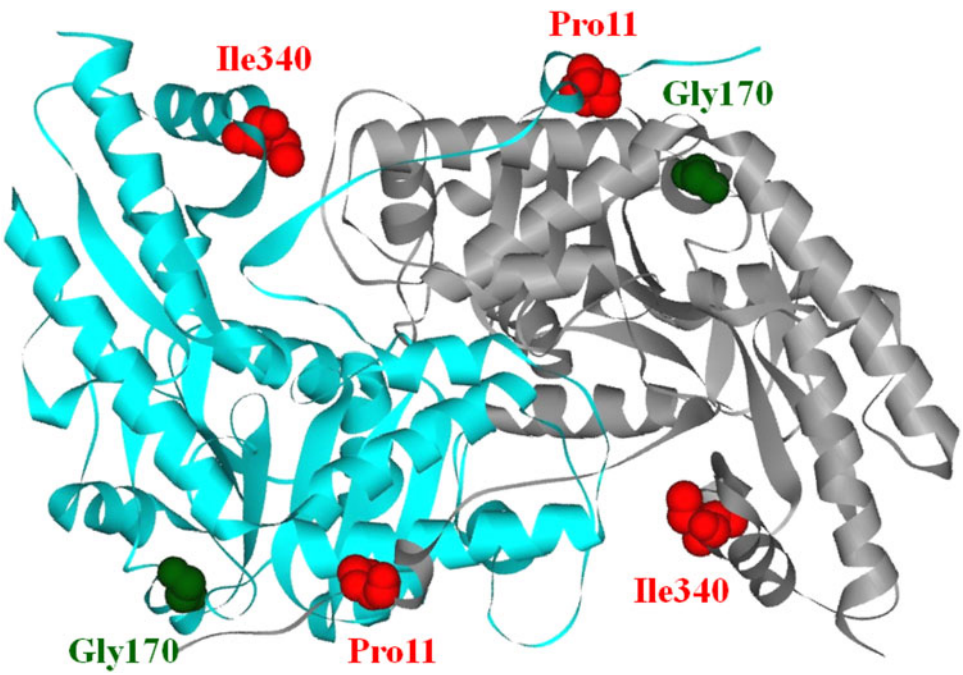

Fig. 1 Localization of the AGT mutations analyzed in our study in the three-dimensional structure of AGT dimer. The residues mutated in the AGT_{LM} variant (P11L/I340M) are shown (in *red* colour in the online version) and also the additional mutation found in the LRM variant (G170R) (shown in *green* colour in the online version). The two monomers are displayed distinctly coloured. The figure was created using the X-ray crystal structure reported by Zhang et al. (PDB code 1H0C; Zhang et al. 2003) and the Discovery Studio Visualizer 2.0 software (Accelrys Software Inc.)

in a mammalian cell-free system shows that AGT_{wt} binds to Hsc70 and Hsp90 proteins under mild acidic conditions but weakly at neutral pH, while the mistargeting variant AGT_{LRM} variant shows strong binding to Hsc70 and Hsp90 at both neutral and acidic pH. Our results provide new insight into the molecular mechanisms involving AGT mitochondrial mistargeting, which might be useful to design new therapies meant to block AGT mitochondrial import either by native state stabilization or specific inhibition of AGT:chaperone interactions.

Materials and methods

Protein expression and purification

JM109 bacterial strains containing plasmids encoding AGT proteins were grown in the presence of ampicillin 0.1 mg/ml to a $OD_{600} = 0.6$ and then induced with 1 mM IPTG for 16–20 h at 28°C. His-AGT was purified from soluble extracts using IMAC-columns (Talon™, ClonTech) as recommended by the manufacturer. Dimeric forms of AGT protein were isolated by size-exclusion chromatography (SEC) in a HiLoad™ 16/60 Superdex™ 200 prep grade column (GE Healthcare) calibrated with molecular mass standards running with Na-Hepes 20 mM, NaCl 200 mM pH 7.4 at 1 ml/min. Holo- and apo-AGT were prepared as described by Cellini et al. (2007) and stored in Na-Hepes 20 mM, NaCl 200 mM pH 7.4 in liquid nitrogen at 5–15 mg/ml. Protein concentration was measured spectrophotometrically using a $\varepsilon_{280(1\ mg/ml)} = 1.069$, calculated based on AGT primary structure (Pace et al. 1995).

Sample preparation

For pH dependent studies, protein stock solutions (in Na-Hepes 20 mM 200 mM pH 7.4) were diluted 50-fold into buffers at specific pH values (adjusted using NaOH or KOH) containing 100 mM of: formic acid (pH 3), acetic acid (pH 4–5.5), NaH_2PO_4 (pH 6–7.5) or Hepes (pH 7–8). All buffers also contained 100 mM NaCl or KCl unless indicated.

Spectroscopic analysis

CD measurements were performed in a Jasco J-810 spectropolarimeter using a 1-mm (far-UV; 5 μM protein subunit) or 5-mm (near-UV; 10 μM protein subunit) path length cuvettes. Fluorescence measurements were performed in PerkinElmer LS50 and LS55 spectrofluorimeters using a 1-cm path length cuvettes and 1 μM protein subunit. Intrinsic emission spectra were recorded by excitation at 280 nm and emission between 300 and 450 nm. ANS fluorescence was measured in the presence of 100 μM ANS by excitation at 380 nm and emission between 425 and 550 nm (in all cases slits were 5 nm). Appropriate blanks in the absence of protein were taken prior to the samples and subtracted. Titrations of apo-AGT with PLP were measured by quenching of intrinsic fluorescence as described (Cellini et al. 2007).

Activity measurements

Specific activities were measured using 1–2 μg of AGT incubated in the corresponding buffer (at different pHs; see above) at 25°C for 1 h and then 40 μM PLP, 10 mM glyoxylate and 40 mM L-alanine were added. Pyruvate formed in the reactions was measured by a coupled NADH:lactate dehydrogenase assay after 2 min reaction at 25°C (Rumsby et al. 1997).

Differential scanning calorimetry

Measurements were performed on a capillary VP-DSC differential scanning calorimeter (MicroCal, GE Healthcare) with a cell volume of 0.135 ml at the indicated scan rates. Temperature ranges were typically 20–80°C (apo-forms) or 20–100°C (holo-forms). Protein samples (~1–20 μM; ~0.05–0.8 mg/ml) were routinely buffer exchanged using PD-10 columns (GE Healthcare) to freshly made and filtered 20 mM Na-Hepes 200 mM pH 7.4 (unless otherwise indicated) and centrifuged prior to the experiments. PLP was added customarily in a 5-fold excess in experiments performed using holo-AGT and incubated in the presence of the protein for at least 4 h at 4°C in the dark prior to experiments.

Experiments performed using holo-AGT forms were shown to be protein-concentration independent, and thus, DSC scans were modeled on the basis of a two-state irreversible model depicted by the following scheme: $N \longrightarrow F$, where N holds for native state and F holds for the final state which cannot fold back to N under the given experimental conditions (Sanchez-Ruiz 1992; Sanchez-Ruiz et al. 1988). Fittings to the two-state irreversible model were performed essentially as described previously (Rodriguez-Larrea et al. 2006). In the case of apo-forms, the protein concentration dependence of the DSC scans prompted us to include non-first-order kinetics in the two-state irreversible model (Sanchez-Ruiz 1992). A detailed description of the models and fitting procedures can be found in the Supplementary information.

Proteolysis

Protein samples (0.5 mg/ml apo-AGT_{wt}) were incubated at pH 7.5 or 4.5 in the presence of 10 mM $CaCl_2$ and variable concentrations of thermolysin at 25°C for 2–60 min.

Reactions were stopped by adding 25 mM EDTA pH 8. Proteolysis was analyzed by SDS-PAGE under reducing conditions using 12% acrylamide gels.

In vitro expression of AGT variants in a cell-free system and interaction with Hsc70 and Hsp90 proteins

Expression in a rabbit reticulocyte cell-free system (TnT system, Promega) was performed at 30°C for 2 h using ^{35}S-Met and hAGT cDNA variants subcloned in pCIneo plasmids (Promega). The reaction was stopped with 100 μg/ml cycloheximide, and 1/25th of the reaction product was set aside for analysis. For immunoprecipitation studies, reaction mixtures were divided into two equal aliquots: one was placed on ice, and the other was brought to pH 4.5 by adding 1/10th volume of 0.1 M sodium acetate. After 1 h incubation at 25°C, 1/3rd volume of 0.1 M Na-Hepes, pH 7.5 was added to both aliquots, to restore neutral pH, prior to immunoprecipitation using antibodies anti-Hsc70 or anti-Hsp90 as previously described (Santana et al. 2003). The immunoprecipitated proteins and the initial TnT products were denatured in Laemmli's buffer and analyzed by SDS-PAGE and fluorography. The immunoprecipitation experiments were repeated three times, the autoradiograms scanned and the fraction of immunoprecipitated AGT protein was normalized to the total amount present in the initial TnT products.

Results

Conformation and function of hAGT variants at physiological pH

Expression analysis of AGT variants in *E. coli* revealed differences in the protein yield as functional dimers, being about 40–50% for AGT_{LM} and 2–5% for AGT_{LRM}, compared to AGTwt qualitatively agreeing with previous studies (Lumb and Danpure. 2000). As shown in Table 1, all three AGT variants behave as dimers of similar apparent sizes as seen by analytical size-exclusion chromatography (SEC) in the protein concentration range used in this study (1–100 μM in subunit). The estimated apparent size for all the forms was 95.2 ± 1.7 kDA, consistent with dimeric forms (87.6 kDa) independently on the presence of PLP bound. In all forms, the three AGT variants displayed similar specific activity when assayed using isolated dimeric forms (Table 1).

Further characterization of dimeric conformations of the AGT variants were performed by circular dichroism (CD) and intrinsic fluorescence emission spectroscopies (Fig. 2). The Far-UV CD spectra for all variants are essentially identical (Fig. 2a) as well as the estimated secondary structure content (compiled in Table 1), with a predominant α-helical conformation (32.7 ± 0.7%, average of all variants). Near-UV–visible CD spectroscopy also showed a characteristic band for PLP bound centered at about 430 nm with similar intensities in all the holo-forms (Fig. 2a inset) arising from the visible absorption band centered at 420 nm of the PLP cofactor placed in an asymmetric protein environment, while all the apo-forms lacked this band in the visible range (Fig. 2a). The intrinsic emission fluorescence spectra of the holo-forms were 3–4-fold lower in intensity at the maximum (at ~340 nm) than in the apo-forms, consistent with fluorescence quenching upon PLP binding (Fig. 2b; Cellini et al. 2007). Titration of the apo-forms with PLP led to a similar ~4-fold decrease in the fluorescence intensity (Fig. 2b; inset), indicating that the holo-forms were essentially saturated with PLP. By monitoring fluorescence quenching in the presence of different PLP concentrations, we estimated similarly high

Table 1 Functional and conformational properties of dimeric holo- and apo-AGT variants

AGT variant	Activity (μmol Pyr mg^{-1} h^{-1})	Apparent size (kDa)[a]	Secondary structure[b]		K_d (PLP) (nM)
			α-Helix	β-Sheet	
Holo					
Wt	1,849 ± 235	94.7 ± 6.0	32.5 ± 1.6	18.5 ± 1.3	N.a.
LM	2,031 ± 207	97.2 ± 7.8	32.6 ± 2.3	18.3 ± 2.4	N.a.
LRM	1,824 ± 172	96.9 ± 6.4	33.1 ± 1.5	17.9 ± 1.2	N.a.
Apo					
Wt	1,426 ± 232	93.1 ± 8.1	33.8 ± 0.3	17.0 ± 0.3	95 ± 29
LM	1,548 ± 240	93.6 ± 7.6	32.6 ± 0.7	18.3 ± 1.0	109 ± 37
LRM	1,702 ± 222	95.6 ± 5.2	31.6 ± 0.9	19.3 ± 1.1	73 ± 26

Data are mean ± SD of at least three independent experiments performed using different protein batches of each variant except for PLP binding affinity where data are mean ± SE from the fitting

[a] Determined by SEC using 1–100 μM protein subunit

[b] Determined from Far-UV CD spectra using the CDNN algorithm (Bohm et al. 1992)

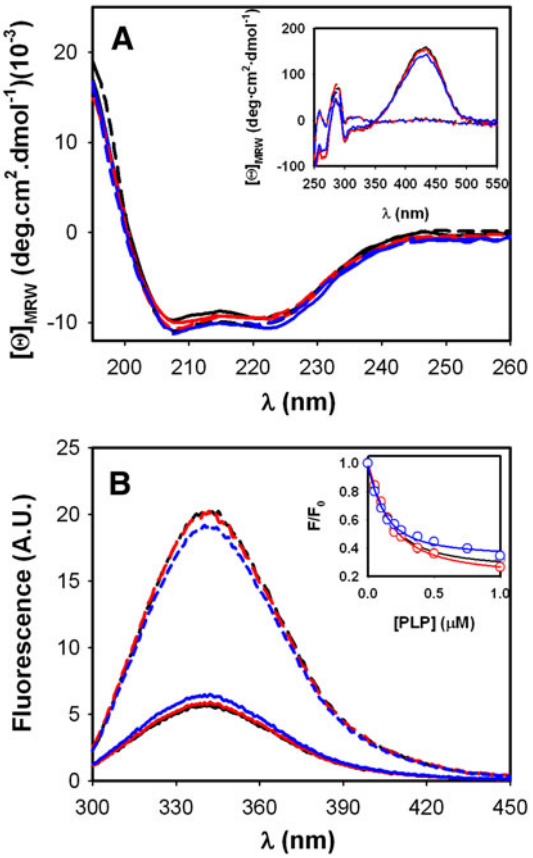

Fig. 2 Conformational properties of AGT dimeric protein variants at pH 7.4. **a** Far-UV CD spectra; *inset* near-UV–visible CD spectra. **b** Emission fluorescence spectra (exc. 280 nm). *Inset* fluorescence titration of apo-AGT proteins. *Continuous lines* are for holo-forms, *dashed lines* for apo-forms. AGT protein variants are displayed coloured in the online version as follows: AGT_{wt} (*black*), AGT_{LM} (*red*) and AGT_{LRM} (*blue*). All the spectroscopic analysis are performed in K-phosphate 20 mM pH 7.4 KCl 100 mM. Experimental temperatures were 25°C

binding affinities for PLP in all three variants (Table 1). Overall, these results indicated that the AGT variants display essentially the same conformational and functional properties of AGT_{wt} but they differently affect the folding efficiency in *E. coli* as expression system.

Thermal unfolding of AGT variants at pH 7.4

We next performed a comparative study on the thermal stability of AGT variants by differential scanning calorimetry (DSC). Under our experimental conditions, thermal unfolding experiments showed a single endothermic transition, displayed complete irreversibility (as the absence of calorimetric signal in reheats stopped after the unfolding transition is complete; Fig. S1 for illustrative examples; the presence of 1 mM TCEP did not improve reversibility) and they were strongly scan-rate dependent (Fig. 3a, b), indicating kinetic control of the thermal unfolding process (Sanchez-Ruiz 1992, 2010; Sanchez-Ruiz et al. 1988). These results indicate that thermal unfolding of both holo- and apo-AGT_{wt} is under kinetic control. We have tested whether a simple two-state kinetic model:

Native AGT dimer → Irreversibly denatured AGT

provides an adequate description of AGT thermal unfolding. The unfolding transitions of holo-AGT_{wt} are essentially independent of protein concentration (Fig. 3c), suggesting that the kinetic process is first-order to good approximation, and that therefore, the unfolding transition state for the irreversible denaturation of holo-AGT_{wt} is dimeric and retains PLP bound. However, apo-AGT_{wt} thermal unfolding significantly depends on protein concentration, suggesting at least partial dissociation in the unfolding transition state for apo-AGT (Fig. 3d).

DSC profiles were fitted using a two-state kinetic model that includes dissociation into μ subunits upon going from the native state to the transition state (see Supplementary information for further details). Fittings were excellent (Figs. 3, 4) and showed internal consistency as the activation energies at different scan rates were very similar, and close to the values obtained from the T_m dependence on the scan rates (Table 2; Fig. S1). As shown by Bevington analyses (Fig. S2), the estimation of the μ values from all fittings is statistically robust. As expected from the essential independence of DSC scan on protein concentration, μ values were close to unity for all three holo-variants (Table 2). For the apo-AGT_{wt} and apo-AGT_{LM} variants, the μ values were higher than unity, and in the case of apo-AGT_{wt}, the average μ value obtained from the fittings was consistent with that obtained from the T_m dependence on the protein concentration (Table 2; Fig. 3d).

It is evident from the experimental DSC scans that PLP binding largely up-shifts the T_m values of all AGT variants ($\sim$25°C), while an individual comparison of both apo- and holo-forms shows a higher T_m for AGT_{wt} than for LM and LRM variants (Table 2; Fig. 4a). The large differences between the calorimetric enthalpies (ΔH_{cal}) of apo- and holo-forms are consistent with a large unfolding heat capacity change (ΔC_p). A plot of the ΔH_{cal} versus T_m (Fig. S3) provides values of 4.0 ± 0.2 kcal mol^{-1} K^{-1} and 173 kcal mol^{-1} for the ΔC_p and $\Delta H_{cal(60°C)}$, respectively. These values are somewhat lower than those predicted for a monomer of 392 residues based on the correlation reported by Robertson and Murphy [5.4 kcal mol^{-1} K^{-1} and 274 kcal mol^{-1}, for ΔC_p and $\Delta H_{cal(60°C)}$, respectively (Robertson and Murphy 1997)], but still indicate that a large fraction of the AGT tertiary structure is disrupted upon thermal unfolding.

Our kinetic analysis based on the two-state irreversible model also allows calculating the unfolding rates for the

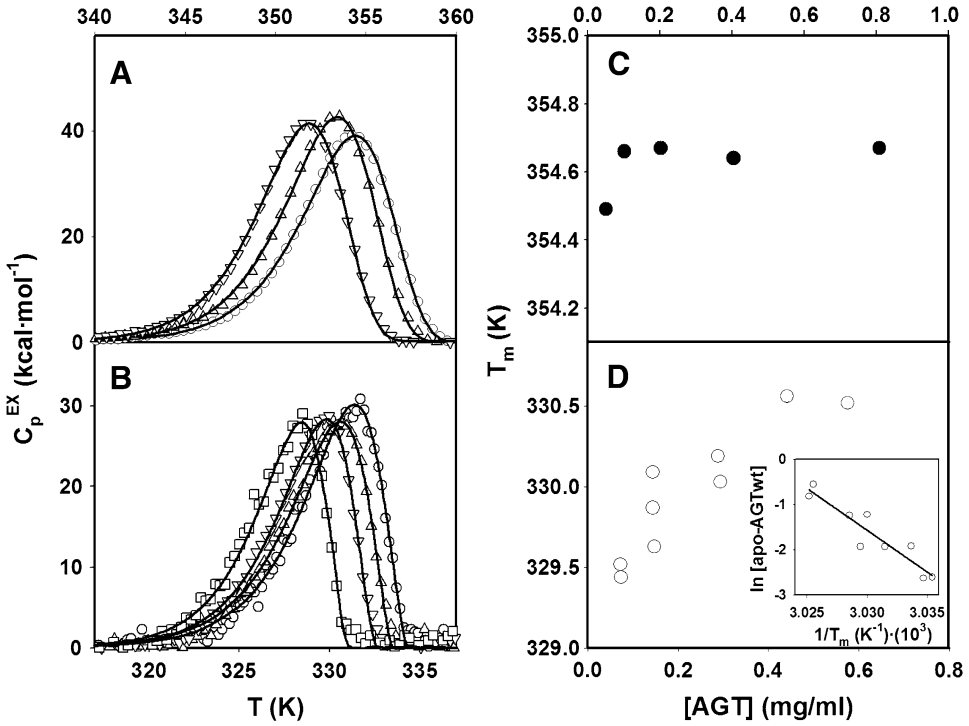

Fig. 3 Thermal unfolding of holo- and apo-AGT_{wt}. Scan rate dependence of the thermal unfolding of holo-AGT_{wt} (**a**) and apo-AGT_{wt} (**b**) using 5 μM monomer, and protein concentration dependence of thermal unfolding for holo-AGT_{wt} (**c**) and apo-AGT_{wt} (**d**). *Lines* in panel **a** show best-fits to a two-state irreversible model without dimer dissociation (protein concentration independent, see panel **c**) while in panel **b**, the model involves dimer dissociation (protein concentration dependent, see panel **d**). The *inset* in panel **d** allows to calculate $\mu = 1.33 \pm 0.18$ for apo-AGT_{wt}. Experiments were performed in Hepes 20 mM NaCl 200 mM pH 7.4. The symbols in panels **a** and **b** represent the different scan rates used: 3 K/min (*circles*), 2 K/min (*up triangles*), 1 K/min (*down triangles*) and 0.5 K/min (*squares*)

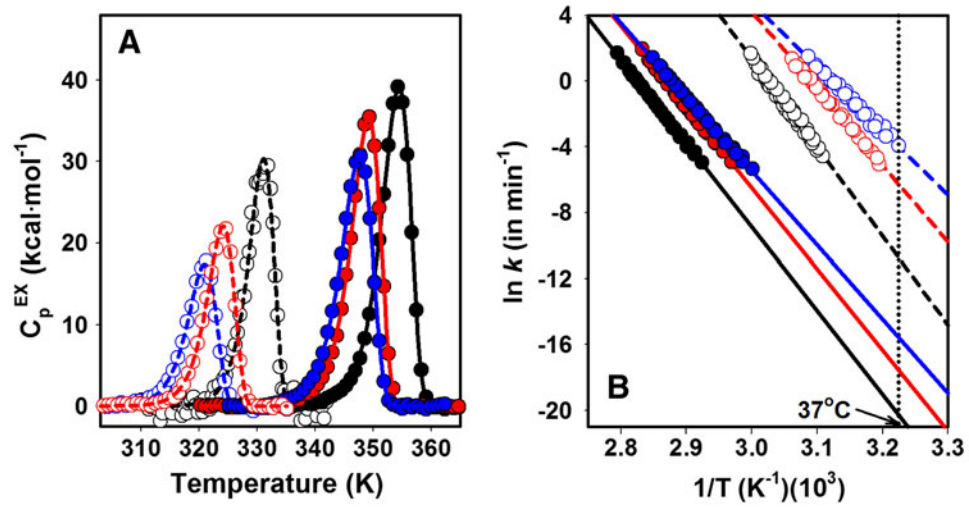

Fig. 4 Thermal unfolding of AGT variants by DSC. **a** Representative DSC traces obtained at 3 K/min and 5 μM protein concentration (in subunit). *Lines* are fits to the corresponding kinetic model. Chemical baselines have been subtracted (as described in supplementary information); **b** Arrhenius plots for the irreversible thermal unfolding of AGT variants. *Closed symbols* are for holo-AGT and *open symbols* for apo-AGT, while *color code* (in the online version) is as in Fig. 2. Experiments were performed in Hepes 20 mM NaCl 200 mM pH 7.4

AGT variants extrapolated to physiological temperatures (Fig. 4b), providing the values compiled in Table 2. All the holo-AGT variants show substantial kinetic stability at physiological temperature (with half lives in the range of years), even though the LM and LRM variants showed decreased kinetic stability in about one and two orders of

Table 2 Stability and kinetic parameters for the irreversible thermal unfolding of dimeric holo and apo-forms of AGT variants

AGT variant	T_m (°C)[a,d]	ΔH_{cal} (kcal/mol)[b,d]	E_a (kcal/mol)[b,d]	k (37°C) (min^{-1})[c]	μ[b,d]
Holo					
Wt	81.3	266 ± 11	106 ± 3	1.55×10^{-9}	0.92 ± 0.02
LM	76.1	250 ± 15	100 ± 1	2.43×10^{-8}	0.99 ± 0.03
LRM	74.5	212 ± 7	92 ± 1	1.77×10^{-7}	0.98 ± 0.01
Apo					
Wt	58.0	157 ± 13	82 ± 5	2.20×10^{-5}	1.35 ± 0.12
LM	51.0	135 ± 12	85 ± 3	1.95×10^{-3}	1.19 ± 0.14
LRM	47.8	121 ± 7	87 ± 6	1.87×10^{-2}	0.94 ± 0.06

[a] Scan rate 3 K/min; 5 μM protein subunit

[b] Average of at least three independent scans at different scan rates

[c] Extrapolated from Arrhenius plot in Fig. 4b

[d] Values obtained using a two-state irreversible model with non-first-order kinetics (see Supplementary material)

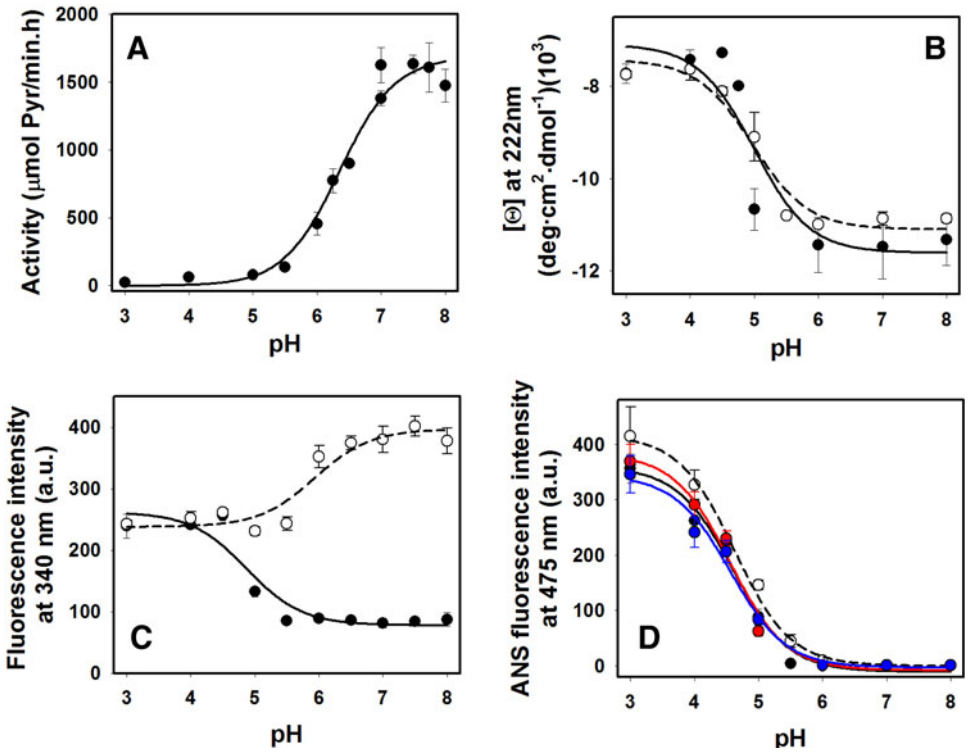

Fig. 5 pH dependence of the activity and conformational properties of AGT. **a** Activity; **b** Far-UV CD; **c** intrinsic fluorescence (exc. 280 nm) and **d** extrinsic fluorescence due to ANS binding (exc. 380 nm). Data are mean ± SD of three independent experiments (**b**–**d**) or two independent experiments each one performed in triplicate (**a**). *Lines*, *symbols* and *colors* are as in Fig. 2. All the experiments were performed using 0.1 M buffer 0.1 M KCl

magnitude, respectively (Table 2). Removal of the bound cofactor largely increases unfolding rates (in about 4–5 orders of magnitude), leading to a remarkably low kinetic stability in the least stable apo-variant at physiological temperature (apo-AGT_{LRM} displays a estimated half-life of ~40 min at 37°C at this protein concentration).

hAGT populates a partially unfolded state at mild acidic pH

The specific activity of holo-AGT_{wt} shows an optimum at pH 7–8 and a progressive decrease at more acidic conditions, with an apparent pK = 6.4 ± 0.1 (Fig. 5a), in agreement with a recent report [(Cellini et al. 2008), obtained using untagged-AGT]. AGT inactivation is highly reversible if the protein is transferred from pH 5.5 to pH 7.5 and incubated for 1 h (~95% of the original activity is recovered). However, AGT samples transferred from pH 3 to pH 7.5 do not recover significant activity (~3% of control activity). As shown in Fig. 5b, both holo- and apo-AGT show a decrease in Far-UV CD signal (about 30% of the signal at neutral pH) at acidic pH, with apparent pK values of 5.0 ± 0.3 and 5.0 ± 0.2, respectively, values somewhat lower than the apparent pK found for the

reversible inactivation process (Fig. 5a), indicating structural changes occur at pH lower than 5.5 which irreversibly inactivate the enzyme. This decrease in Far-UV CD signal does not coincide with any noticeable change in the wavelength of the maximum intrinsic fluorescence emission (with average λ_{max} of 340.0 ± 0.6 and 340.3 ± 1.2 nm, for holo-AGT and apo-AGT, respectively) even though the fluorescence intensities do vary in the mild acidic range (Fig. 5c). Both holo- and apo-AGT_{wt} show a large enhancement in ANS fluorescence at low pH values, and similar ANS binding is observed for AGT_{LM} and AGT_{LRM} in their holo-forms (in all cases, with an apparent pK value of 4.6 ± 0.1; Fig. 5d). Last, SEC experiments at pH 7.5–4.5 show native hydrodynamic behavior above pH 5.5 (consistent with a native dimer), while AGT eluted at the total volume of the column at pH 4.5, suggesting protein interaction with the gel matrix. Interestingly, the spectral properties of both holo- and apo-AGT are remarkably similar at low pHs, also suggesting cofactor release at low pH under the incubation conditions used.

The conformational properties of the unfolding intermediate state described above (high residual secondary structure, non-native enhanced binding of ANS and enhanced ability to interact with the dextran gel matrix) are features often observed in *molten globule* states (Campos and Sancho 2003; Halskau et al. 2009; Liu and Cowan 2009; Polverino de Laureto et al. 2002; Polverino de Laureto et al. 2001). *Molten globules* are also known to be highly flexible and structurally fluctuating protein ensembles. As shown in Fig. S4A, no unfolding thermal transition is evident at pH 4.5 by DSC (in contrast to pH 7.5), which may indicate the absence of significant tertiary interactions at acidic pH [sometimes observed in molten globules thermal unfolding; (Griko and Privalov 1994; Yutani et al. 1992)]. Moreover, partial proteolysis of the full-length apo-AGT by thermolysin at pH 7.5 rapidly leads to the formation of a ~38 kDa band (Fig. S4B), which is completed after 1 h incubation (not shown). This main proteolysis product shows a molecular size of about ~70 kDa (by SEC) that retains over 90% of the native specific activity. In contrast, proteolysis at pH 4.5 leads to the formation of multiple bands of different molecular sizes within a few minutes, indicating that the protease is able to attach to and cleave at multiple sites of the entire protein sequence at this pH, probably due to increased protein flexibility, a behavior also observed previously for other molten globule states (Polverino de Laureto et al. 2002).

Interaction of AGT with Hsc70 and Hsp90 chaperones under native and mildly denaturing conditions

Partially folded states as those described in our work for AGT at mild acidic pH may drive the folding process to the native state and/or constitute kinetic traps that block proper folding (Dobson 2003). In many cases, efficient protein folding in vivo is achieved by interactions of these partially folded states with molecular chaperones (Dobson 2003), which in turn might also deliver proteins to the mitochondrial import machinery (Bukau et al. 2006; Kutik et al. 2007; Young et al. 2003). In order to test whether AGT native and partially folded states would interact with molecular chaperones, we have performed in vitro synthesis of AGT_{wt} and AGT_{LRM} protein in a mammalian cell-free system. The results are summarized in Fig. 6. Upon in vitro synthesis, transfer of both AGT_{wt} and AGT_{LRM} proteins to mild acidic pH leads to significant interaction with Hsc70 and Hsp90 proteins (Fig. 6), showing the ability of these partially folded states to interact with these molecular chaperones. Interestingly, AGT_{LRM} shows similar interaction with Hsc70 and Hsp90 proteins at both pH 4.5 and 7.5, while at pH 7.5 the amount of AGT_{wt} protein bound to these chaperones is very low. These results suggest that AGT_{LRM} protein populates more extensively partially folded states capable of interact with these chaperones, or that they interact in a longer term with Hsc70 and Hsp90 proteins.

Discussion

Proteostasis (protein homeostasis) networks involve multiple cellular interacting agents that modulate protein synthesis, folding, degradation and trafficking (Powers et al. 2009). In this context, it has been proposed that protein energetics in combination with the proteostasis network capacity determine the fate of folded proteins (folding, assembly, aggregation, degradation). Consistent with this model, when a protein "crosses" a certain minimal "proteostasis boundary" (for instance, due to mutations) and exceeds the capacity of the proteostasis network to assist its efficient folding/assembly/transport, the mutant protein become disease-causing (Powers et al. 2009). In this work, we provide evidence on the molecular mechanism underlying the mistargeting phenotype of the AGT_{LRM} protein, a variant known to cause PH1 due to mistargeting to mitochondria instead of peroxisomes. Our results reveal that a combination of decreased kinetic stability of the folded native state and strong kinetic trapping of partially folded forms by interaction with Hsc70 and Hsp90 chaperones may allow delivery of partially folded states of AGT_{LRM} to the mitochondrial import machinery. Therefore, alterations on AGT proteostasis described in this work suggest that AGT stabilizers (pharmacological chaperones) as well as agents that modulate chaperone activities (proteostasis regulators) might be used to correct the trafficking defects described in some PH1-causing variants (ongoing research).

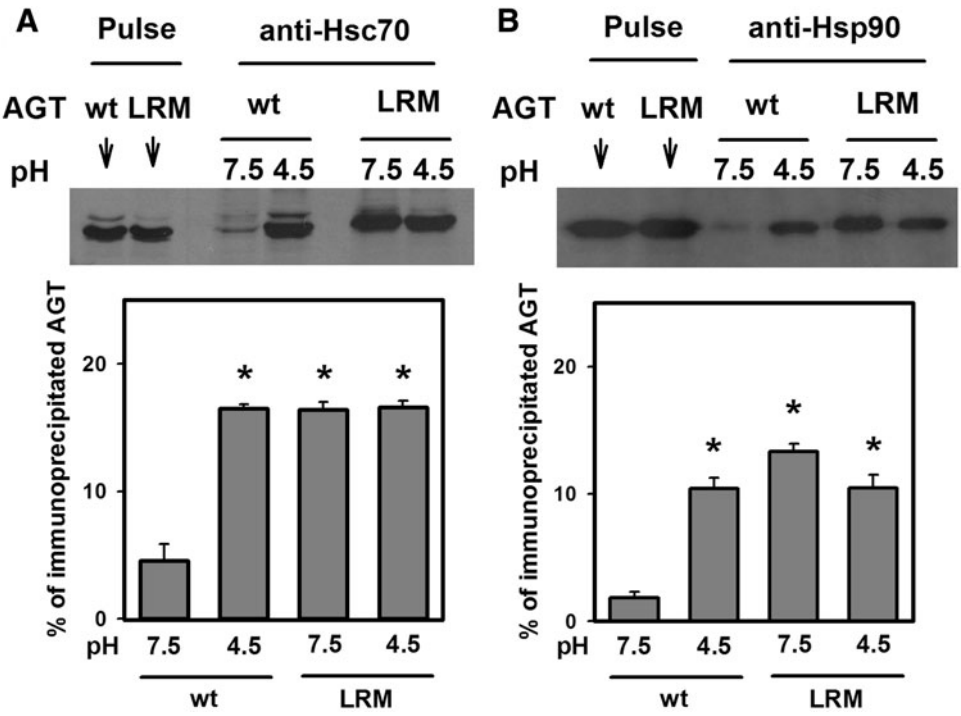

Fig. 6 Interaction between AGT variants and Hsc70 (**a**) and Hsp90 (**b**) proteins under native (pH 7.5) or partially denaturing (pH 4.5) conditions. The autoradiograms shown are representative of three independent experiments in each case. The *panels* show the fraction (mean ± SD from three independent experiments) of initial AGT present in pulse samples (1 μL extract per lane) immunoprecipitated at pH 7.5 or 4.5 (6 μL of extract loaded per lane). Experiments were performed at pH 7.5 (using 0.1 M Na-Hepes) and pH 4.5 (using 0.1 M Na-acetate) in the presence of 0.1 M NaCl. Differences between the means of the different groups were tested by one-way ANOVA (the *asterisks* stand for a statistical significance of $p < 0.01$ compared to the AGT_{wt} at pH 7.5 group)

The AGT_{LRM} variant shows a dramatic decrease in the yield in functional protein upon expression in *E. coli* [(Lumb and Danpure. 2000) and our work]. Nevertheless, we show that folded dimers of AGT_{wt}, AG_{LM} and AGT_{LRM} variants do not substantially differ in their overall conformation, specific activity and binding affinity for PLP. A recent crystallographic study has shown that the mutation G170R only affects locally protein conformation on the *major* allele (Djordjevic et al. 2010). However, we observed a large decrease in AGT_{LRM} and AGT_{LM} protein kinetic stability as seen by DSC analysis based on a two-state irreversible model. This kinetic destabilization is possibly reflecting an increase in the kinetic accessibility of unfolded or partially unfolded states from the native AGT state, unfolded states which may rapidly aggregate, and therefore, are not significantly populated along the thermal transition. Using a simple transition-state theory calculation (Rodriguez-Larrea et al. 2006), the LM and LRM apo-variants are kinetically destabilized by ~2.8 and ~4.2 kcal/mol (at physiological temperature), respectively. On the other hand, PLP binding induces a large kinetic stabilization of all apo-forms, largely exceeding the mutational effect of LM and LRM (6.7 ± 0.7 kcal/mol, average of the three variants). Mutational kinetic destabilization have been recently shown for other PH1 apo-variants such as F152I and G41R on the *minor allele* (Cellini et al. 2009, 2010), but a quantitative comparison with the corresponding holo-forms was not available until now. Moreover, as deduced from our DSC analysis, holo-AGT_{wt} unfolds through a dimeric transition state, while the apo-AGT_{wt} at least partially dissociate in the unfolding transition state. Still, the μ values for apo-AGT_{wt} and apo-AGT_{LM} are smaller than 2, the value expected for a monomeric transition state. One possible explanation is that two kinetic pathways coexist for the irreversible unfolding of these apo-forms (with only of them involving a monomeric transition state), in such a way that the experimental μ values represent the average of both kinetic pathways. Alternatively, the fractional μ value could be viewed as reflecting partial dissociation of the dimer in the unfolding transition state. We must also note that the μ values for the apo-AGT variants seem to decrease as the kinetic stability decreases upon mutation, suggesting that the lower the kinetic stability is the closer the transition state is to be dimeric (or "native-like"). This behavior may be analogous to the movements of the folding/unfolding transition states towards the native state as the native state is destabilized upon mutation that have been previously described [the so-called "Hammond effect" (Matouschek and Fersht 1993; Matouschek et al. 1995)].

The physiological relevance of this kinetic destabilization observed in vitro for AGT_{LRM} is difficult to clarify for the holo-form, since our kinetic analysis predict a high kinetic stability at physiological temperatures for its holo-form, in contrast to its apo-form. However, several lines of evidence support the presence of a significant fraction of AGT in apo-form in vivo, and therefore, a role for the very low kinetic stability of apo-AGT_{LRM} in the mitochondrial mistargeting of this variant in vivo: (1) Total PLP and PMP found in liver is reported be 15–30 nmol/g wet liver in mice, depending on the dietary intake of pyridoxine (Furth-Walker et al. 1990), which represent 60–120 pmol/mg liver protein [considering 250 mg protein/g wet liver; see (Pey et al. 2003)]. AGT activity in human liver is about 6–20 μmol Pyr/h/mg liver protein (Allsop et al. 1987; Wanders et al. 1990) which represents about 1–6 μg of AGT protein/mg liver protein (considering a specific activity of 3,100–6,500 μmol Pyr/h/mg AGT; (Noguchi and Takada 1979; Lumb and Danpure 2000)) or 25–140 pmol AGT subunit/mg liver protein, suggesting that the ratios of total PLP:AGT and PMP:AGT are around 1. Even though these calculations are not meant to quantitatively determine the fraction of AGT present in its apo-state, it is plausible that a significant fraction of AGT in the apo-state may be found in human liver, since PLP and PMP must be shared with other hepatic enzymes. (2) AGT possibly requires the formation of a native apo-enzyme to be able to bind PLP, leading to accumulation to some extent of apo-forms in the cytosol prior to PLP binding. This is consistent with PLP release upon reversible unfolding of dimeric *E. coli* aspartate aminotransferase (Deu and Kirsch 2007) and our data on holo-AGT partially denatured by acidic pH and guanidinium chloride (Fig. 5; Fig. S5); (3) PLP binding kinetics is relatively slow (Fig. S6), and occurs in the same time scale of irreversible unfolding of apo-AGT_{LRM}. At physiological total concentrations of PLP of around 15–30 μM [considering a 1 g/ml density for liver tissue and values of total PLP content in mice liver from (Furth-Walker et al. 1990)], the half-life for PLP binding is expected to be of about $\sim$10–20 min for apo-AGT at 25°C (Fig. S6), which is in the same range of the expected half-life for irreversible unfolding of apo-AGT_{LRM} (about 40 min at 37°C).

Our thermal unfolding analyses do not provide information on the conformational properties of any (partially) unfolded AGT protein states (since they are not significantly populated within the transition), even though our DSC analysis suggest that they would be kinetically more accessible from the native state in the AGT_{LM} and AGT_{LRM} variants. We also show that recombinant AGT_{wt} is capable of adopting such partially unfolded states under moderate acidic pH and also at neutral pH in the presence of moderate guanidinium chloride concentrations (1–2 M GdmHCl; see Fig. S5), indicating that different environmental conditions may induce the formation of these partially unfolded states at relatively low (close to physiological) temperatures. These partially unfolded states display several features classically associated to *molten globule* states (Dobson 1994; Halskau et al. 2009; Liu and Cowan 2009; Polverino de Laureto et al. 2001, 2002), such as high residual secondary structure, solvent exposed hydrophobic regions and enhanced structural flexibility. The role of such partially folded/unfolded states in the folding process may be assisting the protein to find its native fold and/or inhibiting proper folding acting as kinetic traps (Dobson 2003). The low *operational* reversibility of this partial unfolding process under our experimental conditions [even though it would be possible to find very mild refolding conditions where the reversibility is enhanced, such as those described for AGT in (Coulter-Mackie et al. 2005)] suggest a role for molecular chaperones in AGT protein folding in vivo, bypassing adverse parallel reactions such as protein aggregation (Dobson 2003). We show that partially unfolded states triggered by mild acidic pH strongly interact with Hsc70 and Hsp90 chaperones (Fig. 6). We have recently solved the three-dimensional structure of a complex between the bacterial chaperonin, GroEL, and a folding intermediate of another mutant variant (I244T) of the hAGT *minor allele* (AGT_{LTM}), providing evidence for a functional model in which the chaperonin promotes folding of the mutant protein through forced unfolding mechanism (Albert et al. 2010). It is noteworthy that previous works on the human mitochondrial aspartate aminotransferase (hmAAT) have also reported the formation of partially unfolded states at acidic pH which resemble those described herein for hAGT, which do not reactivate when transferred to neutral pH at moderate salt concentrations (Artigues et al. 1994) and are also capable of binding to eukaryotic [Hsc70; (Lain et al. 1994)] and prokaryotic [GroEL; (Mattingly et al. 1995)] chaperones.

The differences between peroxisomal and mitochondrial import machineries have been recognized for a long time to play a role in PH1-associated mitochondrial mistargeting of AGT variants (Prakash and Matouschek 2004). Peroxisomal protein import machinery is characterized by its capacity to import folded and oligomeric proteins containing peroxisomal target signals [PTS; (Brown and Baker 2008)]. On the other hand, classical mitochondrial protein import models involve interactions of a N-terminal presequence in the target protein with the translocase outer membrane (TOM) complex, followed by unfolding and translocation through the membrane pore (Kutik et al. 2007). In the case of proteins with short presequences [35 residues or shorter, as found in hAGT variants; (Danpure 2006)], mitochondrial import rates may be limited by global unfolding rates (Matouschek et al. 1997; Wilcox et al. 2005). Our unfolding

kinetic analysis show that holo-AGT_{LRM} variant considerably speed up AGT irreversible unfolding compared to AGT_{wt} and AGT_{LM} (Table 2). However, aggregation is possibly slower at low (~physiological) temperatures, and additional irreversible processes may compete intracellularly for partially unfolded states, such as mitochondrial import in the case of AGT_{LRM}. From this viewpoint, kinetic destabilization of the AGT_{LRM} native state would contribute to mitochondrial import of this AGT variant. The role of protein:chaperone complexes in mitochondrial import has been acknowledged for different protein systems (Bukau et al. 2006; Kutik et al. 2007; Young et al. 2003; Baker et al. 2007), including hmAAT protein (Artigues et al. 2002). We also show that partially folded states of AGT (especially for the AGT_{LRM}) variant may form complexes with Hsc70 and Hsp90 proteins during the folding reaction in vitro (Fig. 6). Increased steady-state levels of AGT:chaperones complexes might also deliver the protein to the mitochondrial import machinery, speeding up mitochondrial import. The formation of such partially folded AGT:Hsc70 complex, together with the weak MTS induced by the P11L mutation (Danpure 2006) would play a role in the delivery of the partially folded AGT protein to TOM complex and consequently, in mitochondrial mistargeting.

In conclusion, we have described the ability of hAGT to form partially unfolded states resembling a molten globule state and capable of binding to Hsc70 and Hsp90 chaperones under mild denaturing conditions. Moreover, in vitro expressed AGT_{LRM} variants show much higher tendency to interact with those chaperones than the wt protein, possibly due to a combination of decreased kinetic stability of the native state and kinetic trapping of partially folded states. These findings raise additional questions about the local and specific roles of potential interactions between native and partially folded states of AGT with the multiple interacting elements of the

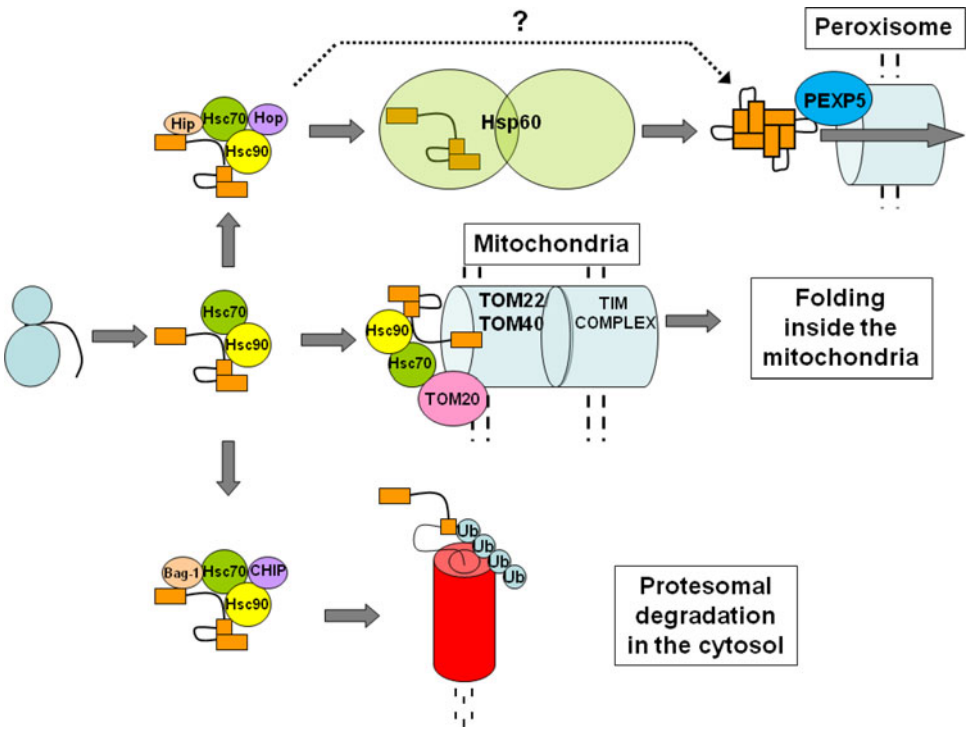

Fig. 7 Potential roles of molecular chaperones and cochaperones (proteostasis network) on the folding, transport and degradation of AGT_{wt} and disease-related variants. Upon translation in the ribosomes, Hsc70 and Hsc90 bind to early folding intermediates (our work; for sake of simplicity the intermediate is displayed monomeric and binds chaperones in a 1:1 stoichiometry). These AGT:chaperone complexes may deliver the non-native AGT to Hsp60 chaperones [see (Cuellar et al. 2008) for Hsp70 delivery of substrates to Hsp60 proteins and (Albert et al. 2010) for the structure of a partially folded AGT stably complexed to Hsp60 proteins] upon interaction with Hip and Hop cochaperones, allowing AGT to reach the native and assembled dimer and to be imported into peroxisomes through interaction with the Pex5P receptor [through direct interaction with the receptor, as shown in the high resolution structure for the AGTfolded dimer:Pex5P receptor complex recently described; PDB code 3IMZ; Wolf and Schliebs, unpublished work, or mediated by an adaptor molecule as suggested by (Huber et al. 2005)], which is likely not efficient in the absence of chaperones (indicated by the *dotted line* and a *question mark*). However, the Hsc70:Hsp90:AGT complex may also allow AGT delivery to the mitochondrial import machinery (upon interaction with TOM20 or TOM70 receptors), or, by interacting with Bag-1 and CHIP cochaperones, may target AGT variants to the ubiquitin-dependent proteasomal degradation. Additional references are found in the main text

proteostasis network (see Fig. 7), such as complexes with Hsc70, Hsp90, and Hsp60 chaperones, their co-chaperones [such as Hip/Hop or CHIP; (Hohfeld et al. 2001; Meimaridou et al. 2009; Albert et al. 2010; Young et al. 2003)], and the effects of small ligands (Hopper et al. 2008; Santana et al. 2003) in determining the final fate of AGT variants. We have initiated experiments using cell-model systems to ascertain the impact of PH1 variants on the AGT proteostasis network, and whether modulation of this network might correct the molecular defects caused by PH1 mutations.

Acknowledgments We want to thank Prof. Aurora Martinez at the University of Bergen for support at the initial stages of this work. This work was supported by grants from the Spanish Ministry of Education (SAF2007-62343 to E.S. and BIO2009–09562 and CSD2009-00088 to J.M.S-R). Angel L. Pey is supported by a Ramon y Cajal research contract from the Spanish Ministry of Science and Innovation (MICINN) and also acknowledges a short-term fellowship from the Federation of European Biochemical Societies (FEBS).

Conflict of interest The authors declare that they have no conflict of interest.

References

Albert A, Yunta C, Arranz R, Pena A, Salido E, Valpuesta JM, Martin-Benito J (2010) Structure of GroEL in complex with an early folding intermediate of alanine glyoxylate aminotransferase. J Biol Chem 285:6371–6376

Allsop J, Jennings PR, Danpure CJ (1987) A new micro-assay for human liver alanine:glyoxylate aminotransferase. Clin Chim Acta 170:187–193

Artigues A, Iriarte A, Martinez-Carrion M (1994) Acid-induced reversible unfolding of mitochondrial aspartate aminotransferase. J Biol Chem 269:21990–21999

Artigues A, Iriarte A, Martinez-Carrion M (2002) Binding to chaperones allows import of a purified mitochondrial precursor into mitochondria. J Biol Chem 277:25047–25055

Baker MJ, Frazier AE, Gulbis JM, Ryan MT (2007) Mitochondrial protein-import machinery: correlating structure with function. Trends Cell Biol 17:456–464

Bohm G, Muhr R, Jaenicke R (1992) Quantitative analysis of protein far UV circular dichroism spectra by neural networks. Protein Eng 5:191–195

Brown LA, Baker A (2008) Shuttles and cycles: transport of proteins into the peroxisome matrix. Mol Membr Biol 25:363–375

Bukau B, Horwich AL (1998) The Hsp70 and Hsp60 chaperone machines. Cell 92:351–366

Bukau B, Weissman J, Horwich A (2006) Molecular chaperones and protein quality control. Cell 125:443–451

Campos LA, Sancho J (2003) The active site of pepsin is formed in the intermediate conformation dominant at mildly acidic pH. FEBS Lett 538:89–95

Cellini B, Bertoldi M, Montioli R, Paiardini A, Borri Voltattorni C (2007) Human wild-type alanine:glyoxylate aminotransferase and its naturally occurring G82E variant: functional properties and physiological implications. Biochem J 408:39–50

Cellini B, Montioli R, Bianconi S, Lopez-Alonso JP, Voltattorni CB (2008) Construction, purification and characterization of untagged human liver alanine-glyoxylate aminotransferase expressed in *Escherichia coli*. Protein Pept Lett 15:153–159

Cellini B, Montioli R, Paiardini A, Lorenzetto A, Voltattorni CB (2009) Molecular insight into the synergism between the minor allele of human liver peroxisomal alanine:glyoxylate aminotransferase and the F152I mutation. J Biol Chem 284:8349–8358

Cellini B, Montioli R, Paiardini A, Lorenzetto A, Maset F, Bellini T, Oppici E, Voltattorni CB (2010) Molecular defects of the glycine 41 variants of alanine glyoxylate aminotransferase associated with primary hyperoxaluria type I. Proc Natl Acad Sci USA 107:2896–2901

Coulter-Mackie MB, Lian Q, Wong SG (2005) Overexpression of human alanine:glyoxylate aminotransferase in *Escherichia coli*: renaturation from guanidine-HCl and affinity for pyridoxal phosphate co-factor. Protein Exp Purif 41:18–26

Cuellar J, Martin-Benito J, Scheres SH, Sousa R, Moro F, Lopez-Vinas E, Gomez-Puertas P, Muga A, Carrascosa JL, Valpuesta JM (2008) The structure of CCT-Hsc70 NBD suggests a mechanism for Hsp70 delivery of substrates to the chaperonin. Nat Struct Mol Biol 15:858–864

Danpure CJ (2006) Primary hyperoxaluria type 1: AGT mistargeting highlights the fundamental differences between the peroxisomal and mitochondrial protein import pathways. Biochim Biophys Acta 1763:1776–1784

Deu E, Kirsch JF (2007) Cofactor-directed reversible denaturation pathways: the cofactor-stabilized *Escherichia coli* aspartate aminotransferase homodimer unfolds through a pathway that differs from that of the apoenzyme. Biochemistry 46:5819–5829

Djordjevic S, Zhang X, Bartlam M, Ye S, Rao Z, Danpure CJ (2010) Structural implications of a G170R mutation of alanine:glyoxylate aminotransferase that is associated with peroxisome-to-mitochondrion mistargeting. Acta Crystallogr Sect F 66:233–236

Dobson CM (1994) Protein folding. Solid evidence for molten globules. Curr Biol 4:636–640

Dobson CM (2003) Protein folding and misfolding. Nature 426:884–890

Furth-Walker B, Leibman D, Smolen A (1990) Relationship between blood, liver and brain pyridoxal phosphate and pyridoxamine phosphate concentrations in mice. J Nutr 120:1338–1343

Griko YV, Privalov PL (1994) Thermodynamic puzzle of apomyoglobin unfolding. J Mol Biol 235:1318–1325

Halskau O, Muga A, Martinez A (2009) Linking new paradigms in protein chemistry to reversible membrane-protein interactions. Curr Protein Pept Sci 10:339–359

Hohfeld J, Cyr DM, Patterson C (2001) From the cradle to the grave: molecular chaperones that may choose between folding and degradation. EMBO Rep 2:885–890

Hopper ED, Pittman AM, Fitzgerald MC, Tucker CL (2008) In vivo and in vitro examination of stability of primary hyperoxaluria-associated human alanine:glyoxylate aminotransferase. J Biol Chem 283:30493–30502

Huber PA, Birdsey GM, Lumb MJ, Prowse DT, Perkins TJ, Knight DR, Danpure CJ (2005) Peroxisomal import of human alanine:glyoxylate aminotransferase requires ancillary targeting information remote from its C terminus. J Biol Chem 280:27111–27120

Kutik S, Guiard B, Meyer HE, Wiedemann N, Pfanner N (2007) Cooperation of translocase complexes in mitochondrial protein import. J Cell Biol 179:585–591

Lain B, Iriarte A, Martinez-Carrion M (1994) Dependence of the folding and import of the precursor to mitochondrial aspartate aminotransferase on the nature of the cell-free translation system. J Biol Chem 269:15588–15596

Liu Y, Cowan JA (2009) Iron-sulfur cluster biosynthesis: characterization of a molten globule domain in human NFU. Biochemistry 48:7512–7518

Lumb MJ, Danpure CJ (2000) Functional synergism between the most common polymorphism in human alanine:glyoxylate aminotransferase and four of the most common disease-causing mutations. J Biol Chem 275:36415–36422

Martinez A, Calvo AC, Teigen K, Pey AL (2008) Rescuing proteins of low kinetic stability by chaperones and natural ligands: phenylketonuria, a case study. Prog Mol Biol Transl Sci 83:89–134

Matouschek A, Fersht AR (1993) Application of physical organic chemistry to engineered mutants of proteins: Hammond postulate behavior in the transition state of protein folding. Proc Natl Acad Sci USA 90:7814–7818

Matouschek A, Otzen DE, Itzhaki LS, Jackson SE, Fersht AR (1995) Movement of the position of the transition state in protein folding. Biochemistry 34:13656–13662

Matouschek A, Azem A, Ratliff K, Glick BS, Schmid K, Schatz G (1997) Active unfolding of precursor proteins during mitochondrial protein import. EMBO J 16:6727–6736

Mattingly JR Jr, Iriarte A, Martinez-Carrion M (1995) Homologous proteins with different affinities for groEL. The refolding of the aspartate aminotransferase isozymes at varying temperatures. J Biol Chem 270:1138–1148

Meimaridou E, Gooljar SB, Chapple JP (2009) From hatching to dispatching: the multiple cellular roles of the Hsp70 molecular chaperone machinery. J Mol Endocrinol 42:1–9

Motley A, Lumb MJ, Oatey PB, Jennings PR, De Zoysa PA, Wanders RJ, Tabak HF, Danpure CJ (1995) Mammalian alanine/glyoxylate aminotransferase 1 is imported into peroxisomes via the PTS1 translocation pathway. Increased degeneracy and context specificity of the mammalian PTS1 motif and implications for the peroxisome-to-mitochondrion mistargeting of AGT in primary hyperoxaluria type 1. J Cell Biol 131:95–109

Noguchi T, Takada Y (1979) Peroxisomal localization of alanine:glyoxylate aminotransferase in human liver. Arch Biochem Biophys 196:645–647

Pace CN, Vajdos F, Fee L, Grimsley G, Gray T (1995) How to measure and predict the molar absorption coefficient of a protein. Protein Sci 4:2411–2423

Pey A, Saborido A, Blazquez I, Delgado J, Megias A (2003) Effect of prolonged stanozolol treatment on antioxidant enzyme activities, oxidative stress markers, and heat shock protein HSP72 levels in rat liver. J Steroid Biochem Mol Biol 87:269–277

Polverino de Laureto P, Vinante D, Scaramella E, Frare E, Fontana A (2001) Stepwise proteolytic removal of the beta subdomain in alpha-lactalbumin. The protein remains folded and can form the molten globule in acid solution. Eur J Biochem 268:4324–4333

Polverino de Laureto P, Frare E, Gottardo R, Van Dael H, Fontana A (2002) Partly folded states of members of the lysozyme/lactalbumin superfamily: a comparative study by circular dichroism spectroscopy and limited proteolysis. Protein Sci 11:2932–2946

Powers ET, Morimoto RI, Dillin A, Kelly JW, Balch WE (2009) Biological and chemical approaches to diseases of proteostasis deficiency. Annu Rev Biochem 78:959–991

Prakash S, Matouschek A (2004) Protein unfolding in the cell. Trends Biochem Sci 29:593–600

Purdue PE, Allsop J, Isaya G, Rosenberg LE, Danpure CJ (1991) Mistargeting of peroxisomal L-alanine:glyoxylate aminotransferase to mitochondria in primary hyperoxaluria patients depends upon activation of a cryptic mitochondrial targeting sequence by a point mutation. Proc Natl Acad Sci USA 88:10900–10904

Robertson AD, Murphy KP (1997) Protein structure and the energetics of protein stability. Chem Rev 97:1251–1268

Rodriguez-Larrea D, Minning S, Borchert TV, Sanchez-Ruiz JM (2006) Role of solvation barriers in protein kinetic stability. J Mol Biol 360:715–724

Rumsby G, Weir T, Samuell CT (1997) A semiautomated alanine:glyoxylate aminotransferase assay for the tissue diagnosis of primary hyperoxaluria type 1. Ann Clin Biochem 34:400–404

Sanchez-Ruiz JM (1992) Theoretical analysis of Lumry-Eyring models in differential scanning calorimetry. Biophys J 61:921–935

Sanchez-Ruiz JM (2010) Protein kinetic stability. Biophys Chem 148:1–15

Sanchez-Ruiz JM, Lopez-Lacomba JL, Cortijo M, Mateo PL (1988) Differential scanning calorimetry of the irreversible thermal denaturation of thermolysin. Biochemistry 27:1648–1652

Santana A, Salido E, Torres A, Shapiro LJ (2003) Primary hyperoxaluria type 1 in the Canary Islands: a conformational disease due to I244T mutation in: the P11L-containing alanine:glyoxylate aminotransferase. Proc Natl Acad Sci USA 100:7277–7282

Wanders RJ, Ruiter J, Van Roermund CW, Schutgens RB, Ofman R, Jurriaans S, Tager JM (1990) Human liver L-alanine-glyoxylate aminotransferase: characteristics and activity in controls and hyperoxaluria type I patients using a simple spectrophotometric method. Clin Chim Acta 189:139–144

Wilcox AJ, Choy J, Bustamante C, Matouschek A (2005) Effect of protein structure on mitochondrial import. Proc Natl Acad Sci USA 43:15435–15440

Williams EL, Acquaviva C, Amoroso A, Chevalier F, Coulter-Mackie M, Monico CG, Giachino D, Owen T, Robbiano A, Salido E, Waterham H, Rumsby G (2009) Primary hyperoxaluria type 1: update and additional mutation analysis of the AGXT gene. Hum Mutat 30:910–917

Young JC, Hoogenraad NJ, Hartl FU (2003) Molecular chaperones Hsp90 and Hsp70 deliver preproteins to the mitochondrial import receptor Tom70. Cell 112:41–50

Yutani K, Ogasahara K, Kuwajima K (1992) Absence of the thermal transition in apo-alpha-lactalbumin in the molten globule state. A study by differential scanning microcalorimetry. J Mol Biol 228:347–350

Zhang X, Roe SM, Hou Y, Bartlam M, Rao Z, Pearl LH, Danpure CJ (2003) Crystal structure of alanine:glyoxylate aminotransferase and the relationship between genotype and enzymatic phenotype in primary hyperoxaluria type 1. J Mol Biol 331:643–652